

Observation of a cross-section enhancement near mass threshold in $e^+e^- \rightarrow \Lambda\bar{\Lambda}$

M. Ablikim,¹ M. N. Achasov,^{9,d} S. Ahmed,¹⁴ X. C. Ai,¹ O. Albayrak,⁵ M. Albrecht,⁴ D. J. Ambrose,⁴⁵ A. Amoroso,^{50a,50c}
 F. F. An,¹ Q. An,^{47,38} J. Z. Bai,¹ O. Bakina,²³ R. Baldini Ferroli,^{20a} Y. Ban,³¹ D. W. Bennett,¹⁹ J. V. Bennett,⁵ N. Berger,²²
 M. Bertani,^{20a} D. Bettoni,^{21a} J. M. Bian,⁴⁴ F. Bianchi,^{50a,50c} E. Boger,^{23,b} I. Boyko,²³ R. A. Briere,⁵ H. Cai,⁵² X. Cai,^{1,38}
 O. Cakir,^{41a} A. Calcaterra,^{20a} G. F. Cao,^{1,42} S. A. Cetin,^{41b} J. Chai,^{50c} J. F. Chang,^{1,38} G. Chelkov,^{23,b,c} G. Chen,¹
 H. S. Chen,^{1,42} J. C. Chen,¹ M. L. Chen,^{1,38} S. Chen,⁴² S. J. Chen,²⁹ X. Chen,^{1,38} X. R. Chen,²⁶ Y. B. Chen,^{1,38}
 X. K. Chu,³¹ G. Cibinetto,^{21a} H. L. Dai,^{1,38} J. P. Dai,^{34,h} A. Dbeyssi,¹⁴ D. Dedovich,²³ Z. Y. Deng,¹ A. Denig,²²
 I. Denysenko,²³ M. Destefanis,^{50a,50c} F. De Mori,^{50a,50c} Y. Ding,²⁷ C. Dong,³⁰ J. Dong,^{1,38} L. Y. Dong,^{1,42} M. Y. Dong,^{1,38,42}
 Z. L. Dou,²⁹ S. X. Du,⁵⁴ P. F. Duan,¹ J. Z. Fan,⁴⁰ J. Fang,^{1,38} S. S. Fang,^{1,42} X. Fang,^{47,38} Y. Fang,¹ R. Farinelli,^{21a,21b}
 L. Fava,^{50b,50c} S. Fegan,²² F. Feldbauer,²² G. Felici,^{20a} C. Q. Feng,^{47,38} E. Fioravanti,^{21a} M. Fritsch,^{22,14} C. D. Fu,¹ Q. Gao,¹
 X. L. Gao,^{47,38} Y. Gao,⁴⁰ Z. Gao,^{47,38} I. Garzia,^{21a} K. Goetzen,¹⁰ L. Gong,³⁰ W. X. Gong,^{1,38} W. Gradl,²² M. Greco,^{50a,50c}
 M. H. Gu,^{1,38} Y. T. Gu,¹² Y. H. Guan,¹ A. Q. Guo,¹ L. B. Guo,²⁸ R. P. Guo,¹ Y. Guo,¹ Y. P. Guo,²² Z. Haddadi,²⁵
 A. Hafner,²² S. Han,⁵² X. Q. Hao,¹⁵ F. A. Harris,⁴³ K. L. He,^{1,42} F. H. Heinsius,⁴ T. Held,⁴ Y. K. Heng,^{1,38,42} T. Holtmann,⁴
 Z. L. Hou,¹ C. Hu,²⁸ H. M. Hu,^{1,42} T. Hu,^{1,38,42} Y. Hu,¹ G. S. Huang,^{47,38} J. S. Huang,¹⁵ X. T. Huang,³³ X. Z. Huang,²⁹
 Z. L. Huang,²⁷ T. Hussain,⁴⁹ W. Ikegami Andersson,⁵¹ Q. Ji,¹ Q. P. Ji,¹⁵ X. B. Ji,^{1,42} X. L. Ji,^{1,38} L. W. Jiang,⁵²
 X. S. Jiang,^{1,38,42} X. Y. Jiang,³⁰ J. B. Jiao,³³ Z. Jiao,¹⁷ D. P. Jin,^{1,38,42} S. Jin,^{1,42} T. Johansson,⁵¹ A. Julin,⁴⁴
 N. Kalantar-Nayestanaki,²⁵ X. L. Kang,¹ X. S. Kang,³⁰ M. Kavatsyuk,²⁵ B. C. Ke,⁵ P. Kiese,²² R. Kliemt,¹⁰ B. Kloss,²²
 O. B. Kolcu,^{41b,f} B. Kopf,⁴ M. Kornicer,⁴³ A. Kupsc,⁵¹ W. Kühn,²⁴ J. S. Lange,²⁴ M. Lara,¹⁹ P. Larin,¹⁴ H. Leithoff,²²
 C. Leng,^{50c} C. Li,⁵¹ Cheng Li,^{47,38} D. M. Li,⁵⁴ F. Li,^{1,38} F. Y. Li,³¹ G. Li,¹ H. B. Li,^{1,42} H. J. Li,¹ J. C. Li,¹ Jin Li,³² K. Li,¹³
 K. Li,³³ Lei Li,³ P. L. Li,^{47,38} P. R. Li,^{42,7} Q. Y. Li,³³ T. Li,³³ W. D. Li,^{1,42} W. G. Li,¹ X. L. Li,³³ X. N. Li,^{1,38} X. Q. Li,³⁰
 Y. B. Li,² Z. B. Li,³⁹ H. Liang,^{47,38} Y. F. Liang,³⁶ Y. T. Liang,²⁴ G. R. Liao,¹¹ D. X. Lin,¹⁴ B. Liu,^{34,h} B. J. Liu,¹
 C. X. Liu,¹ D. Liu,^{47,38} F. H. Liu,³⁵ Fang Liu,¹ Feng Liu,⁶ H. B. Liu,¹² H. H. Liu,¹⁶ H. H. Liu,¹ H. M. Liu,^{1,42} J. Liu,¹
 J. B. Liu,^{47,38} J. P. Liu,⁵² J. Y. Liu,¹ K. Liu,⁴⁰ K. Y. Liu,²⁷ L. D. Liu,³¹ P. L. Liu,^{1,38} Q. Liu,⁴² S. B. Liu,^{47,38} X. Liu,²⁶
 Y. B. Liu,³⁰ Y. Y. Liu,³⁰ Z. A. Liu,^{1,38,42} Zhiqing Liu,²² H. Loehner,²⁵ Y. F. Long,³¹ X. C. Lou,^{1,38,42} H. J. Lu,¹⁷
 J. G. Lu,^{1,38} Y. Lu,¹ Y. P. Lu,^{1,38} C. L. Luo,²⁸ M. X. Luo,⁵³ T. Luo,⁴³ X. L. Luo,^{1,38} X. R. Lyu,⁴² F. C. Ma,²⁷ H. L. Ma,¹
 L. L. Ma,³³ M. M. Ma,¹ Q. M. Ma,¹ T. Ma,¹ X. N. Ma,³⁰ X. Y. Ma,^{1,38} Y. M. Ma,³³ F. E. Maas,¹⁴ M. Maggiora,^{50a,50c}
 Q. A. Malik,⁴⁹ Y. J. Mao,³¹ Z. P. Mao,¹ S. Marcello,^{50a,50c} J. G. Messchendorp,²⁵ G. Mezzadri,^{21b} J. Min,^{1,38} T. J. Min,¹
 R. E. Mitchell,¹⁹ X. H. Mo,^{1,38,42} Y. J. Mo,⁶ C. Morales Morales,¹⁴ G. Morello,^{20a} N. Yu. Muchnoi,^{9,d} H. Muramatsu,⁴⁴
 P. Musiol,⁴ Y. Nefedov,²³ F. Nerling,¹⁰ I. B. Nikolaev,^{9,d} Z. Ning,^{1,38} S. Nisar,⁸ S. L. Niu,^{1,38} X. Y. Niu,¹ S. L. Olsen,³²
 Q. Ouyang,^{1,38,42} S. Pacetti,^{20b} Y. Pan,^{47,38} M. Papenbrock,⁵¹ P. Patteri,^{20a} M. Pelizaeus,⁴ H. P. Peng,^{47,38} K. Peters,^{10,g}
 J. Pettersson,⁵¹ J. L. Ping,²⁸ R. G. Ping,^{1,42} R. Poling,⁴⁴ V. Prasad,¹ H. R. Qi,² M. Qi,²⁹ S. Qian,^{1,38} C. F. Qiao,⁴²
 L. Q. Qin,³³ N. Qin,⁵² X. S. Qin,¹ Z. H. Qin,^{1,38} J. F. Qiu,¹ K. H. Rashid,^{49,i} C. F. Redmer,²² M. Ripka,²² G. Rong,^{1,42}
 Ch. Rosner,¹⁴ X. D. Ruan,¹² A. Sarantsev,^{23,e} M. Savrié,^{21b} C. Schnier,⁴ K. Schoenning,⁵¹ W. Shan,³¹ M. Shao,^{47,38}
 C. P. Shen,² P. X. Shen,³⁰ X. Y. Shen,^{1,42} H. Y. Sheng,¹ W. M. Song,¹ X. Y. Song,¹ S. Sosio,^{50a,50c} S. Spataro,^{50a,50c}
 G. X. Sun,¹ J. F. Sun,¹⁵ S. S. Sun,^{1,42} X. H. Sun,¹ Y. J. Sun,^{47,38} Y. Z. Sun,¹ Z. J. Sun,^{1,38} Z. T. Sun,¹⁹ C. J. Tang,³⁶
 X. Tang,¹ I. Tapan,^{41c} E. H. Thorndike,⁴⁵ M. Tiemens,²⁵ I. Uman,^{41d} G. S. Varner,⁴³ B. Wang,³⁰ B. L. Wang,⁴² D. Wang,³¹
 D. Y. Wang,³¹ K. Wang,^{1,38} L. L. Wang,¹ L. S. Wang,¹ M. Wang,³³ P. Wang,¹ P. L. Wang,¹ W. Wang,^{1,38} W. P. Wang,^{47,38}
 X. F. Wang,⁴⁰ Y. Wang,³⁷ Y. D. Wang,¹⁴ Y. F. Wang,^{1,38,42} Y. Q. Wang,²² Z. Wang,^{1,38} Z. G. Wang,^{1,38} Z. H. Wang,^{47,38}
 Z. Y. Wang,¹ Zongyuan Wang,¹ T. Weber,²² D. H. Wei,¹¹ P. Weidenkaff,²² S. P. Wen,¹ U. Wiedner,⁴ M. Wolke,⁵¹
 L. H. Wu,¹ L. J. Wu,¹ Z. Wu,^{1,38} L. Xia,^{47,38} L. G. Xia,⁴⁰ Y. Xia,¹⁸ D. Xiao,¹ H. Xiao,⁴⁸ Z. J. Xiao,²⁸ Y. G. Xie,^{1,38}
 Y. H. Xie,⁶ Q. L. Xiu,^{1,38} G. F. Xu,¹ J. J. Xu,¹ L. Xu,¹ Q. J. Xu,¹³ Q. N. Xu,⁴² X. P. Xu,³⁷ L. Yan,^{50a,50c} W. B. Yan,^{47,38}
 W. C. Yan,^{47,38} Y. H. Yan,¹⁸ H. J. Yang,^{34,h} H. X. Yang,¹ L. Yang,⁵² Y. X. Yang,¹¹ M. Ye,^{1,38} M. H. Ye,⁷ J. H. Yin,¹
 Z. Y. You,³⁹ B. X. Yu,^{1,38,42} C. X. Yu,³⁰ J. S. Yu,²⁶ C. Z. Yuan,^{1,42} Y. Yuan,¹ A. Yuncu,^{41b,a} A. A. Zafar,⁴⁹ Y. Zeng,¹⁸
 Z. Zeng,^{47,38} B. X. Zhang,¹ B. Y. Zhang,^{1,38} C. C. Zhang,¹ D. H. Zhang,¹ H. H. Zhang,³⁹ H. Y. Zhang,^{1,38} J. Zhang,¹
 J. J. Zhang,¹ J. L. Zhang,¹ J. Q. Zhang,¹ J. W. Zhang,^{1,38,42} J. Y. Zhang,¹ J. Z. Zhang,^{1,42} K. Zhang,¹ L. Zhang,¹
 S. Q. Zhang,³⁰ X. Y. Zhang,³³ Y. Zhang,¹ Y. Zhang,¹ Y. H. Zhang,^{1,38} Y. N. Zhang,⁴² Y. T. Zhang,^{47,38} Yu Zhang,⁴²
 Z. H. Zhang,⁶ Z. P. Zhang,⁴⁷ Z. Y. Zhang,⁵² G. Zhao,¹ J. W. Zhao,^{1,38} J. Y. Zhao,¹ J. Z. Zhao,^{1,38} Lei Zhao,^{47,38} Ling Zhao,¹
 M. G. Zhao,³⁰ Q. Zhao,¹ Q. W. Zhao,¹ S. J. Zhao,⁵⁴ T. C. Zhao,¹ Y. B. Zhao,^{1,38} Z. G. Zhao,^{47,38} A. Zhemchugov,^{23,b}
 B. Zheng,^{48,14} J. P. Zheng,^{1,38} W. J. Zheng,³³ Y. H. Zheng,⁴² B. Zhong,²⁸ L. Zhou,^{1,38} X. Zhou,⁵² X. K. Zhou,^{47,38}
 X. R. Zhou,^{47,38} X. Y. Zhou,¹ K. Zhu,¹ K. J. Zhu,^{1,38,42} S. Zhu,¹ S. H. Zhu,⁴⁶ X. L. Zhu,⁴⁰ Y. C. Zhu,^{47,38} Y. S. Zhu,^{1,42}
 Z. A. Zhu,^{1,42} J. Zhuang,^{1,38} L. Zotti,^{50a,50c} B. S. Zou,¹ and J. H. Zou¹

(BESIII Collaboration)

- ¹*Institute of High Energy Physics, Beijing 100049, People's Republic of China*
²*Beihang University, Beijing 100191, People's Republic of China*
³*Beijing Institute of Petrochemical Technology, Beijing 102617, People's Republic of China*
⁴*Bochum Ruhr-University, D-44780 Bochum, Germany*
⁵*Carnegie Mellon University, Pittsburgh, Pennsylvania 15213, USA*
⁶*Central China Normal University, Wuhan 430079, People's Republic of China*
⁷*China Center of Advanced Science and Technology, Beijing 100190, People's Republic of China*
⁸*COMSATS Institute of Information Technology, Lahore, Defence Road, Off Raiwind Road, 54000 Lahore, Pakistan*
⁹*G.I. Budker Institute of Nuclear Physics SB RAS (BINP), Novosibirsk 630090, Russia*
¹⁰*GSI Helmholtzcentre for Heavy Ion Research GmbH, D-64291 Darmstadt, Germany*
¹¹*Guangxi Normal University, Guilin 541004, People's Republic of China*
¹²*Guangxi University, Nanning 530004, People's Republic of China*
¹³*Hangzhou Normal University, Hangzhou 310036, People's Republic of China*
¹⁴*Helmholtz Institute Mainz, Johann-Joachim-Becher-Weg 45, D-55099 Mainz, Germany*
¹⁵*Henan Normal University, Xinxiang 453007, People's Republic of China*
¹⁶*Henan University of Science and Technology, Luoyang 471003, People's Republic of China*
¹⁷*Huangshan College, Huangshan 245000, People's Republic of China*
¹⁸*Human University, Changsha 410082, People's Republic of China*
¹⁹*Indiana University, Bloomington, Indiana 47405, USA*
^{20a}*INFN Laboratori Nazionali di Frascati, I-00044, Frascati, Italy*
^{20b}*INFN and University of Perugia, I-06100, Perugia, Italy*
^{21a}*INFN Sezione di Ferrara, I-44122, Ferrara, Italy*
^{21b}*University of Ferrara, I-44122, Ferrara, Italy*
²²*Johannes Gutenberg University of Mainz, Johann-Joachim-Becher-Weg 45, D-55099 Mainz, Germany*
²³*Joint Institute for Nuclear Research, 141980 Dubna, Moscow region, Russia*
²⁴*Justus-Liebig-Universitaet Giessen, II. Physikalisches Institut, Heinrich-Buff-Ring 16, D-35392 Giessen, Germany*
²⁵*KVI-CART, University of Groningen, NL-9747 AA Groningen, The Netherlands*
²⁶*Lanzhou University, Lanzhou 730000, People's Republic of China*
²⁷*Liaoning University, Shenyang 110036, People's Republic of China*
²⁸*Nanjing Normal University, Nanjing 210023, People's Republic of China*
²⁹*Nanjing University, Nanjing 210093, People's Republic of China*
³⁰*Nankai University, Tianjin 300071, People's Republic of China*
³¹*Peking University, Beijing 100871, People's Republic of China*
³²*Seoul National University, Seoul 151-747, Korea*
³³*Shandong University, Jinan 250100, People's Republic of China*
³⁴*Shanghai Jiao Tong University, Shanghai 200240, People's Republic of China*
³⁵*Shanxi University, Taiyuan 030006, People's Republic of China*
³⁶*Sichuan University, Chengdu 610064, People's Republic of China*
³⁷*Soochow University, Suzhou 215006, People's Republic of China*
³⁸*State Key Laboratory of Particle Detection and Electronics, Beijing 100049, Hefei 230026, People's Republic of China*
³⁹*Sun Yat-Sen University, Guangzhou 510275, People's Republic of China*
⁴⁰*Tsinghua University, Beijing 100084, People's Republic of China*
^{41a}*Ankara University, 06100 Tandogan, Ankara, Turkey*
^{41b}*Istanbul Bilgi University, 34060 Eyup, Istanbul, Turkey*
^{41c}*Uludag University, 16059 Bursa, Turkey*
^{41d}*Near East University, Nicosia, North Cyprus, Mersin 10, Turkey*
⁴²*University of Chinese Academy of Sciences, Beijing 100049, People's Republic of China*
⁴³*University of Hawaii, Honolulu, Hawaii 96822, USA*
⁴⁴*University of Minnesota, Minneapolis, Minnesota 55455, USA*
⁴⁵*University of Rochester, Rochester, New York 14627, USA*
⁴⁶*University of Science and Technology Liaoning, Anshan 114051, People's Republic of China*
⁴⁷*University of Science and Technology of China, Hefei 230026, People's Republic of China*
⁴⁸*University of South China, Hengyang 421001, People's Republic of China*
⁴⁹*University of the Punjab, Lahore 54590, Pakistan*

^{50a}University of Turin, I-10125 Turin, Italy^{50b}University of Eastern Piedmont, I-15121 Alessandria, Italy^{50c}INFN, I-10125 Turin, Italy⁵¹Uppsala University, Box 516, SE-75120 Uppsala, Sweden⁵²Wuhan University, Wuhan 430072, People's Republic of China⁵³Zhejiang University, Hangzhou 310027, People's Republic of China⁵⁴Zhengzhou University, Zhengzhou 450001, People's Republic of China

(Received 1 October 2017; published 28 February 2018)

The process $e^+e^- \rightarrow \Lambda\bar{\Lambda}$ is studied using data samples at $\sqrt{s} = 2.2324, 2.400, 2.800$ and 3.080 GeV collected with the BESIII detector operating at the BEPCII collider. The Born cross section is measured at $\sqrt{s} = 2.2324$ GeV, which is 1.0 MeV above the $\Lambda\bar{\Lambda}$ mass threshold, to be $305 \pm 45_{-36}^{+66}$ pb, where the first uncertainty is statistical and the second systematic. The cross section near threshold is larger than that expected from theory, which predicts the cross section to vanish at threshold. The Born cross sections at $\sqrt{s} = 2.400, 2.800$ and 3.080 GeV are measured and found to be consistent with previous experimental results, but with improved precision. Finally, the corresponding effective electromagnetic form factors of Λ are deduced.

DOI: 10.1103/PhysRevD.97.032013

I. INTRODUCTION

Electromagnetic form factors (FFs) are important observables for probing the inner structure of hadrons and for understanding the strong interaction. The timelike FFs are mostly measured by electron-positron colliding experiments [1]. The Born cross section for the process $e^+e^- \rightarrow B\bar{B}$ via one-photon exchange, where B is a spin $1/2$ baryon, can be expressed in terms of the electric and magnetic FFs G_E and G_M ,

$$\sigma^B(s) = \frac{4\pi\alpha^2 C\beta}{3s} \left[|G_M(s)|^2 + \frac{2m_B^2 c^4}{s} |G_E(s)|^2 \right]. \quad (1)$$

Here, $\alpha = 1/137.036$ is the fine-structure constant, $\beta = \sqrt{1 - 4m_B^2 c^4/s}$ is the velocity, c is the speed of light, s is the square of the center-of-mass (c.m.) energy, and m_B is the mass of the baryon. The Coulomb correction factor C [2,3], accounting for the electromagnetic interaction of charged pointlike fermion pairs in the final state, is 1.0 for pairs of neutral baryons and $y/(1 - e^{-y})$ with $y = \pi\alpha(1 + \beta^2)/\beta$ for pairs of charged baryons. The effective FF defined by

$$|G| \equiv \sqrt{\frac{|G_M(s)|^2 + (2m_B^2 c^4/s)|G_E(s)|^2}{1 + 2m_B^2 c^4/s}} \quad (2)$$

is proportional to the square root of the baryon pair production cross section.

Experimentally, there have been many studies on the nucleon pair production cross sections and the timelike nucleon FFs in the past decades [4–13]. Unusual behavior in the near-threshold region has been observed for both $e^+e^- \rightarrow p\bar{p}$ and $e^+e^- \rightarrow n\bar{n}$ cross sections [8,10,13]. Compared with neutrons, the production cross section and FFs of hyperons are however hardly explored [14–16]. The BABAR experiment measured the hyperon final states of $\Lambda\bar{\Lambda}$ [15] with significantly larger uncertainties compared to the proton case. The cross section of $e^+e^- \rightarrow \Lambda\bar{\Lambda}$ in a wide c.m. energy region from threshold to $\sqrt{s} = 2.27$ GeV was measured to be $204 \pm 60 \pm 20$ pb, which indicates a possible nonvanishing cross section at threshold. Recently, the BESIII experiment has observed a nonzero cross section near the $\Lambda_c^+ \bar{\Lambda}_c^-$ production threshold in the process $e^+e^- \rightarrow \Lambda_c^+ \bar{\Lambda}_c^-$ [17]. The unexpected features of baryon pair production near threshold have driven many theoretical interests [18], including scenarios that

^aAlso at Bogazici University, 34342 Istanbul, Turkey.^bAlso at the Moscow Institute of Physics and Technology, Moscow 141700, Russia.^cAlso at the Functional Electronics Laboratory, Tomsk State University, Tomsk 634050, Russia.^dAlso at the Novosibirsk State University, Novosibirsk 630090, Russia.^eAlso at the NRC “Kurchatov Institute”, PNPI, 188300 Gatchina, Russia.^fAlso at Istanbul Arel University, 34295 Istanbul, Turkey.^gAlso at Goethe University Frankfurt, 60323 Frankfurt am Main, Germany.^hAlso at Key Laboratory for Particle Physics, Astrophysics and Cosmology, Ministry of Education; Shanghai Key Laboratory for Particle Physics and Cosmology; Institute of Nuclear and Particle Physics, Shanghai 200240, People's Republic of China.ⁱGovernment College Women University, Sialkot 51310, Punjab, Pakistan.

Published by the American Physical Society under the terms of the Creative Commons Attribution 4.0 International license. Further distribution of this work must maintain attribution to the author(s) and the published article's title, journal citation, and DOI. Funded by SCOAP³.

invoke $B\bar{B}$ bound states or unobserved meson resonances. It was also interpreted as an attractive Coulomb interaction on the constituent quark level in Ref. [19]. In order to properly test the hypotheses, a precision measurement of $e^+e^- \rightarrow \Lambda\bar{\Lambda}$ very close to $\Lambda\bar{\Lambda}$ mass threshold is needed.

In this paper, we present a study of process $e^+e^- \rightarrow \Lambda\bar{\Lambda}$ at c.m. energy $\sqrt{s} = 2.2324$ GeV, which is 1.0 MeV above the $\Lambda\bar{\Lambda}$ mass threshold, with two decay modes reconstructed, $\Lambda \rightarrow p\pi^-$, $\bar{\Lambda} \rightarrow \bar{p}\pi^+$ (referred to as mode I) and $\bar{\Lambda} \rightarrow \bar{n}\pi^0$, $\Lambda \rightarrow X$ (referred to as mode II, where X represents the inclusive decay of Λ). Besides, measurements on the process $e^+e^- \rightarrow \Lambda\bar{\Lambda}$ at c.m. energies $\sqrt{s} = 2.400, 2.800, \text{ and } 3.080$ GeV are given with improved precision compared with previous experiments.

II. THE BESIII EXPERIMENT AND THE DATA SETS

The collision data were taken with the BESIII spectrometer at BEPCII. BEPCII is a double-ring e^+e^- collider running at c.m. energies between 2.0–4.6 GeV and reaches a peak luminosity of $1.0 \times 10^{33} \text{ cm}^{-2} \text{ s}^{-1}$ at a c.m. energy of 3770 MeV. The cylindrical BESIII detector has an effective geometrical acceptance of 93% of 4π and divides into a barrel section and two end caps. It contains a small cell, helium-based (60% He, 40% C₃H₈) main drift chamber (MDC) which provides momentum measurement of charged particles with a resolution of 0.5% at a momentum of 1 GeV/c in a magnetic field of 1 Tesla. The energy loss measurement (dE/dx) provided by the MDC has a resolution better than 6%. A time-of-flight system (TOF) consisting of 5-cm-thick plastic scintillators can measure the flight time of charged particles with a time resolution of 80 ps in the barrel and 110 ps in the end caps. An electromagnetic calorimeter (EMC) consisting of 6240 CsI (TI) in a cylindrical structure and two end caps is used to measure the energies of photons and electrons. The energy resolution of the EMC is 2.5% in the barrel and 5.0% in the end caps for photon/electron of 1 GeV energy. The position resolution of the EMC is 6 mm in the barrel and 9 mm in the end caps. A detailed description of the detector and its performance can be found in Ref. [20].

A GEANT4-based [21] Monte Carlo (MC) simulation software package, BOOST [22] is used to generate the signal and background MC samples. The signal process of $e^+e^- \rightarrow \Lambda\bar{\Lambda}$ at $\sqrt{s} = 2.2324$ GeV is generated uniformly in phase space (PHSP) since G_E equals to G_M at threshold by definition [9]. The corresponding correction factor is calculated by taking the higher-order processes with one radiative photon in the final states and the energy spread of collider beams into consideration, where the energy spread is inversely proportional to the beam energy, to be 0.48 MeV from a scaling at J/ψ peak. The subsequent decays of $\Lambda \rightarrow p\pi^-$, $\bar{\Lambda} \rightarrow \bar{p}\pi^+$ for mode I, and $\bar{\Lambda} \rightarrow \bar{n}\pi^0$, $\Lambda \rightarrow X$ for mode II are generated with EVTGEN [23]. The

signal process of $e^+e^- \rightarrow \Lambda\bar{\Lambda}$ at $\sqrt{s} = 2.400, 2.800$ and 3.080 GeV is generated with the software package CONEXC [24], which includes correction factors for higher-order processes with one radiative photon. Simulated samples of the QED background processes $e^+e^- \rightarrow l^+l^-$ ($l = e, \mu$) and $e^+e^- \rightarrow \gamma\gamma$ are generated with BABAYAGA [25]. The generic (“inclusive”) MC samples for hadronic final states from e^+e^- collision are generated with LUNDAREA [26].

III. RECONSTRUCTION OF $e^+e^- \rightarrow \Lambda\bar{\Lambda}$ AT $\sqrt{s} = 2.2324$ GeV

The process $e^+e^- \rightarrow \Lambda\bar{\Lambda}$ at $\sqrt{s} = 2.2324$ GeV is selected via two decay modes, with the final state topologies $p\bar{p}\pi^+\pi^-$ and $\bar{n}\pi^0X$. Due to the near-threshold production and small PHSP in $\Lambda(\bar{\Lambda})$ decays, the nucleon and antinucleon in the final state are difficult to detect. Thus it is impossible to fully reconstruct the final states. Instead, we employ an indirect search for the antiproton in mode I and search for mono-energetic π^0 in mode II, respectively.

For mode I, the low momentum pions from signal final states can be detected directly. A good charged track must have a polar angle θ within $|\cos\theta| < 0.93$ and have a point of closest approach to the interaction point (IP) in the plane perpendicular to the beam, V_{xy} , within 1 cm and along the beam direction, V_z , within 10 cm. The combined information of specific ionisation (dE/dx) and the time-of-flight (TOF) system is used to calculate particle identification (PID) probabilities for the pion, kaon and proton hypotheses, and the particle type with the highest probability is assigned to the track. The candidate events are required to have two good charged tracks identified as one positive and one negative pion, and the momentum of the charged pions is required to be within [0.08, 0.11] GeV/c, as expected from $\Lambda(\bar{\Lambda})$ decay.

The antiproton annihilates from signal final states in the interaction with nucleons of detector materials, mostly in the beam pipe, and produces secondary particles. The distribution of the largest V_{xy} of all tracks apart from the two good charged pions in an event, V_r , as shown in Fig. 1(a), shows an enhancement around 3 cm, which is the distance from the IP to the beam pipe. After applying the above selection criteria, the inclusive background processes in our MC data sample do not contribute to the enhancement. Besides, based on a study of pion momentum sidebands, which are the events located in [0.15, 0.18] GeV/c of pion momentum, there is no peaking background around 3 cm in the V_r distribution. The number of signal events for mode I is extracted by fitting the V_r distribution, where the signal is described by the MC shape, the background is described by the sideband of the π momentum as it is consistent with the distribution from inclusive background processes.

For mode II, at most one good charged track is allowed and at least three neutral candidates are required. Neutral

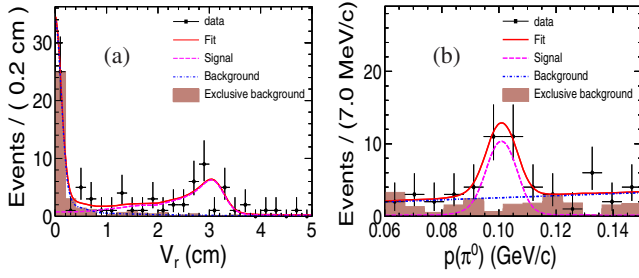


FIG. 1. (a) Fitted V_r distribution for mode I and (b) fitted $p(\pi^0)$ for mode II. The dots with error bars are data, the solid curves (red) are the fit results, the dashed curves (pink) show the signals, the dash-dot curves (blue) show the backgrounds and the shaded histograms are the summed background from exclusive background process which mainly stem from hadronic final states for mode I, hadronic final states and beam-associated background.

candidates are required to have a minimum energy of 25 MeV in the barrel region or 50 MeV in the end-cap region. To eliminate showers produced by charged particles, the neutral candidates are required to have no associated charged tracks within 10° . The most energetic shower is assumed to be a \bar{n} and others to be photons, motivated by MC simulations, since the \bar{n} annihilates with material in electromagnetic calorimeter (EMC) and produces several secondary particles with total energy up to $2m_n$ GeV, where m_n is the mass of neutron from the Particle Data Group (PDG) [27]. A π^0 candidate is identified by a one-constrained (1C) kinematic fit on π^0 mass applied to each photon pair. The energy asymmetry $|E_{\gamma_1} - E_{\gamma_2}|/p_{\pi^0}$ is required to be less than $0.95c$. Furthermore, the angle between the momentum directions of the π^0 and \bar{n} candidates is required to be larger than 140° . If there are several photon pair combinations, the one giving the smallest χ^2_{1C} is identified as the π^0 candidate. To improve the signal-to-background ratio, only events with $\chi^2_{1C} < 20$ are accepted.

After the preliminary selection for mode II, most of the background events from QED processes can be removed. The inclusive hadronic final states with multiple π^0 s and the beam-associated background events [28] are the dominant background sources. A dedicated data sample collected with BESIII with noncolliding beams is used to study the beam-associated background and is described in Ref. [9]. To separate the signal from the background, mainly to distinguish between \bar{n} and γ , the boosted decision tree (BDT) technique [29] is used in this analysis. The signal events are generated with a PHSP generator. The background events are mixtures of hadronic final states and separated-beam events, where the number of hadronic final states is normalized according to the luminosity, and the number of separated-beam events is normalized to the remaining number of events in data. Separate sets of BDTs are built with eight discriminating variables. All input variables are EMC-related and are shown in Table I,

TABLE I. The variables used in the BDT classifier, ranked by the importance.

Rank	Variable	Importance
1	Energy deposition within 40° cone	2.4×10^{-1}
2	Deposited energy	2.0×10^{-1}
3	Deposit of energy seed	1.3×10^{-1}
4	Number of hits within 40° cone	1.1×10^{-1}
5	Number of hits	1.0×10^{-1}
6	Lateral moment	9.3×10^{-2}
7	Second moment	7.6×10^{-2}
8	Deposition shape [30]	5.4×10^{-2}

together with their normalized importance values. An optimal classifier requirement is applied for the BDT output. The distribution of π^0 momentum in data and remaining background after the full selection is shown in Fig. 1(b), where a clear enhancement can be observed around 0.1 GeV/c. An unbinned maximum likelihood fit is performed to determine the number of signal events, where the signal is described by the MC shape convoluted with a Gaussian function, and the background is described by a linear function which appears to give a good description for the background.

The Born cross section of the process $e^+e^- \rightarrow \Lambda\bar{\Lambda}$ is determined from

$$\sigma^B = \frac{N_{\text{obs}}}{\mathcal{L}_{\text{int}}\epsilon(1+\delta)\mathcal{B}}, \quad (3)$$

where \mathcal{L}_{int} is the integrated luminosity, ϵ is the detection efficiency obtained from the signal MC sample, and $1+\delta$ is the radiative correction factor, determined by taking the energy spread and initial state radiation (ISR) photon emission and the vacuum polarization into account. \mathcal{B} is the product of decay branching fractions of intermediate states $\Lambda \rightarrow p\pi^-$ and $\bar{\Lambda} \rightarrow \bar{p}\pi^+$ for mode I, $\bar{\Lambda} \rightarrow \bar{n}\pi^0$, $\Lambda \rightarrow X$ and $\pi^0 \rightarrow \gamma\gamma$ for mode II.

Several sources of systematic uncertainties are considered for the determination of the cross section at $\sqrt{s} = 2.2324$ GeV. The uncertainties for reconstruction of low momentum pions for mode I are studied with $J/\psi \rightarrow p\bar{p}\pi^+\pi^-$. The differences of the efficiencies between data and MC are taken as the uncertainties, which give 12.3% for tracking and 1.0% for PID. The uncertainty of the V_r selection in mode I is also studied from the $J/\psi \rightarrow p\bar{p}\pi^+\pi^-$ process. The recoil momentum of $p\pi^+\pi^-$ is required to be within [0.08, 0.12] GeV/c to match the kinematics of the $\bar{\Lambda}$ decay. The efficiency is defined as the number of events with V_r less than 5 cm to the number of events with the recoil mass of $p\pi^+\pi^-$ lying in the antiproton mass region. This uncertainty is estimated to be 0.3%. The uncertainties of \bar{n} and π^0 selection for mode II are studied in the processes, to be 2.2% and 2.3%,

respectively. The uncertainty associated with the BDT output requirement for mode II is estimated by selecting \bar{n} sample from process $J/\psi \rightarrow p\bar{n}\pi^-$. The efficiency is obtained by applying the same classifier on data and MC, and the difference of 4.8% is taken as the uncertainty. The uncertainty due to the fit procedure is investigated by replacing the background shape with an inclusive MC distribution and varying the fit range, and the uncertainties are found to be 4.6% and 8.8% for modes I and II. The uncertainty of the ISR correction is studied by changing the cross section line shape of $e^+e^- \rightarrow \Lambda\bar{\Lambda}$ in the MC generator and then taking the difference of ${}_{+18.5}^{-3.6}\%$ in the obtained ISR correction factor as the uncertainty. The uncertainty due to the energy spread correction is 2.0% by taking an alternative energy spread value from another $\psi(3686)$ scan. From a measurement of J/ψ meson parameters [31], there is a nominal energy measurement uncertainty, 0.59 MeV, by comparing the mass of reconstructed J/ψ meson with the mass from PDG. Since the two data sets are collected in the same data-taking period, we treat the uncertainty of energy measurement in this analysis to be the same as J/ψ . By interpolating the line shape with c.m. energy value, the difference on $\epsilon(1+\delta)$, 3.9%, is taken as the uncertainty from nominal c.m. energy measurement. The uncertainty of the trigger efficiency is 1.0% for mode II [32]. The uncertainty of the integral luminosity is 1.0%, as determined from large-angle Bhabha events [33]. Assuming all the sources of systematic uncertainty are independent, the total uncertainties are obtained by adding the individual contributions in quadrature, to be ${}_{-14.4}^{+23.2}\%$ and ${}_{-12.6}^{+22.1}\%$ for modes I and II, respectively.

The systematic uncertainty in the effective FF $|G|$ can be derived from Eq. (2). It is half of that of the Born cross section for the uncertainty sources not related with c.m. energy. For the uncertainty from nominal c.m. energy measurement and energy spread, due to the rapid variation of the velocity β versus the c.m. energy near threshold, large uncertainties are taken into consideration, to be ${}_{-9.3}^{+22.6}\%$ for energy shift and ${}_{-9.7}^{+15.2}\%$ for energy spread, respectively.

IV. RECONSTRUCTION OF $e^+e^- \rightarrow \Lambda\bar{\Lambda}$ AT OTHER ENERGY POINTS

The analysis at c.m. energies $\sqrt{s} = 2.400, 2.800$ and 3.080 GeV is straightforward since full reconstruction of the final state $p\bar{p}\pi^+\pi^-$ is feasible. Four good charged tracks with V_{xy} within 10 cm and V_z within 30 cm, identified as one proton-antiproton pair and one pion pair ($\pi^+\pi^-$) are required. Candidates for $\Lambda(\bar{\Lambda})$ are reconstructed with proton and pion tracks. A secondary vertex fit is performed and the track parameters are used to obtain the invariant mass $M_{p\pi^-}(M_{\bar{p}\pi^+})$. The mass window requirement $|M_{p\pi^-} - M_\Lambda| < 0.01$ GeV/ c^2 is used to select $\Lambda(\bar{\Lambda})$ candidates, where M_Λ is the nominal mass of Λ from the PDG [27].

Further, c.m. energy dependent requirements on the opening angle between Λ and $\bar{\Lambda}$ in the center-of-mass system, $\theta_{\Lambda\bar{\Lambda}} > 170^\circ, 176^\circ, 178^\circ$ at $\sqrt{s} = 2.400, 2.800, 3.080$ GeV are applied.

The background of the $e^+e^- \rightarrow \Lambda\bar{\Lambda}$ channel either comes from non- Λ background or Λ peaking background. The non- Λ background is studied from the two-dimensional sideband of $M_{p\pi^-}$ and $M_{\bar{p}\pi^+}$. The sideband regions $1.084 < M_{p\pi^-/\bar{p}\pi^+} < 1.104$ GeV/ c^2 are defined to investigate the potential background without Λ or $\bar{\Lambda}$ in the final states. The Λ peaking background is studied from the exclusive processes, $e^+e^- \rightarrow \Sigma^0\bar{\Sigma}^0$, $e^+e^- \rightarrow \Lambda\bar{\Sigma}^0$ and $e^+e^- \rightarrow \Xi^0\bar{\Xi}^0$. After applying the same selection criteria for the MC samples of these background channels with luminosity normalized, the numbers of surviving background events are found to be negligible.

With the selection criteria applied, the ratios of the $\Lambda\bar{\Lambda}$ invariant mass to c.m. energy, $M_{\Lambda\bar{\Lambda}}/\sqrt{s}$, are shown in Fig. 2, between data and signal MC. Since the number of background events in the peaks can be neglected, we take the number of counts in the range of $0.98 < M_{\Lambda\bar{\Lambda}}/\sqrt{s} < 1.02$ as signal events, N_{obs} .

The Born cross sections of the process $e^+e^- \rightarrow \Lambda\bar{\Lambda}$ at $\sqrt{s} = 2.400, 2.800$ and 3.080 GeV are determined by Eq. (3). The detection efficiency ϵ is determined from MC. The electromagnetic FF ratio, $|G_E/G_M|$, has an impact on the angular distribution of $\Lambda(\bar{\Lambda})$. To address the dependency of the angular distribution of the produced baryon, the detection efficiency is evaluated with the MC samples by sampling the baryon angular distribution with $(1 + \cos^2\theta)$ and $(1 - \cos^2\theta)$, where θ is the polar angle of Λ , corresponding to the $|G_E| = 0$ and $|G_M| = 0$, respectively. The nominal detection efficiency is the average of these efficiencies.

Various sources of systematic uncertainties in the cross section measurements at $\sqrt{s} = 2.400, 2.800$ and 3.080 GeV have been studied. The uncertainty from reconstruction of $\Lambda(\bar{\Lambda})$ and the mass window requirement is determined to be 4.5%, as determined by a control sample of $J/\psi \rightarrow pK^-\bar{\Lambda} + \text{c.c.}$ The unknown angular distribution of the $\Lambda/\bar{\Lambda}$ introduces an additional uncertainty

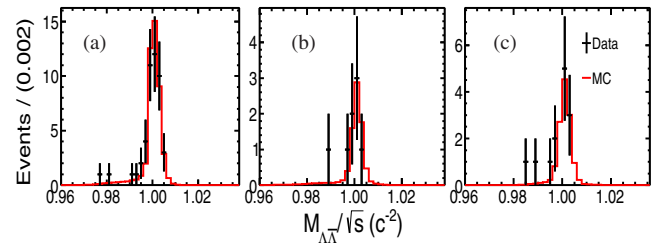


FIG. 2. Ratio of the $\Lambda\bar{\Lambda}$ invariant mass to c.m. energy, $M_{\Lambda\bar{\Lambda}}/\sqrt{s}$, at $\sqrt{s} =$ (a) 2.400 GeV, (b) 2.800 GeV and (c) 3.080 GeV. Dots with error bars are data and the solid curves (red) are the MC simulated events.

TABLE II. The measured Born cross sections, σ^B . The subscripts 1, 2 and c denote mode I, mode II and the combined result. The first uncertainties are statistical and the second systematic.

\sqrt{s} (GeV)	\mathcal{L}_{int} (pb^{-1})	N_{obs}	$\epsilon(1+\delta)$ (%)	σ^B (pb)	$ G $ ($\times 10^{-2}$)
2.2324 ₁	2.63	43 ± 7	12.9	$312 \pm 51^{+72}_{-45}$	
2.2324 ₂	2.63	22 ± 6	8.25	$288 \pm 96^{+64}_{-36}$	
2.2324 _c				$305 \pm 45^{+66}_{-36}$	$61.9 \pm 4.6^{+18.1}_{-9.0}$
2.400	3.42	45 ± 7	25.3	$128 \pm 19 \pm 18$	$12.7 \pm 0.9 \pm 0.9$
2.800	3.75	8 ± 3	36.1	$14.8 \pm 5.2 \pm 1.9$	$4.10 \pm 0.72 \pm 0.26$
3.080	30.73	13 ± 4	24.5	$4.2 \pm 1.2 \pm 0.5$	$2.29 \pm 0.33 \pm 0.14$

in the efficiency. This uncertainty is estimated by taking half of the difference between the two extremes $(1 + \cos^2\theta)$ and $(1 - \cos^2\theta)$ and is within the range 10.8%~12.7%, depending on the c.m. energy. The uncertainty from the ISR correction factor is estimated by varying the input cross section line shape of $e^+e^- \rightarrow \Lambda\bar{\Lambda}$ within uncertainty, and is in the range 2.2%~4.0% depending on c.m. energy. The uncertainty of integrated luminosity is 1.0% [33]. The uncertainties are assumed to be uncorrelated and combined in quadrature, giving in total of 13.0%~14.0% for the cross section measurements at $\sqrt{s} = 2.400, 2.800$ and 3.080 GeV.

V. RESULTS AND CONCLUSION

The resulting Born cross section and the effective FFs of Λ in the timelike region, defined in Eq. (2), at $\sqrt{s} = 2.2324, 2.400, 2.800$ and 3.080 GeV are summarized in Table II. The results at $\sqrt{s} = 2.2324$ GeV from modes I and II are combined taking into account the correlation between the uncertainties of the two decay modes [34,35].

A comparison of the Born cross sections and the effective FFs of the process $e^+e^- \rightarrow \Lambda\bar{\Lambda}$ with previous experimental results is illustrated in Fig. 3, with the mass of $\Lambda\bar{\Lambda}$ pair relative to the its threshold. For better resolution at

$\sqrt{s} = 2.2324$ GeV, a zoomed-in result in the near-threshold region is inserted in each plot. Our results are consistent with previous experiments, but with improved precision. A phenomenological fit, according to the expectation that the cross section should be proportional to the PHSP factor times a perturbative QCD (pQCD) driven energy power [36], is also given in Fig. 3. The anomalous behavior differing from the pQCD prediction at threshold is observed.

In summary, based on an integrated luminosity of 2.63 pb^{-1} data collected at $\sqrt{s} = 2.2324$ GeV, which is 1.0 MeV above the $\Lambda\bar{\Lambda}$ mass threshold, we present a measurement of the process $e^+e^- \rightarrow \Lambda\bar{\Lambda}$. The Born cross section at $\sqrt{s} = 2.2324$ GeV is determined to be $305 \pm 45^{+66}_{-36}$ pb, where the first uncertainty is statistical and the second systematic. The result is larger than the traditional theory expectation for neutral baryon pairs, which predicts a vanishing cross section at threshold according to Eq. (1). The observed threshold enhancement implies a more complicated underlying physics scenario. The Born cross sections of process $e^+e^- \rightarrow \Lambda\bar{\Lambda}$ are also measured at $\sqrt{s} = 2.400, 2.800$ and 3.080 GeV, and are in good agreement with *BABAR* and *DM2*'s results [14,15], but with improved precision. Furthermore, the effective electromagnetic FFs of Λ are presented at each c.m. energy.

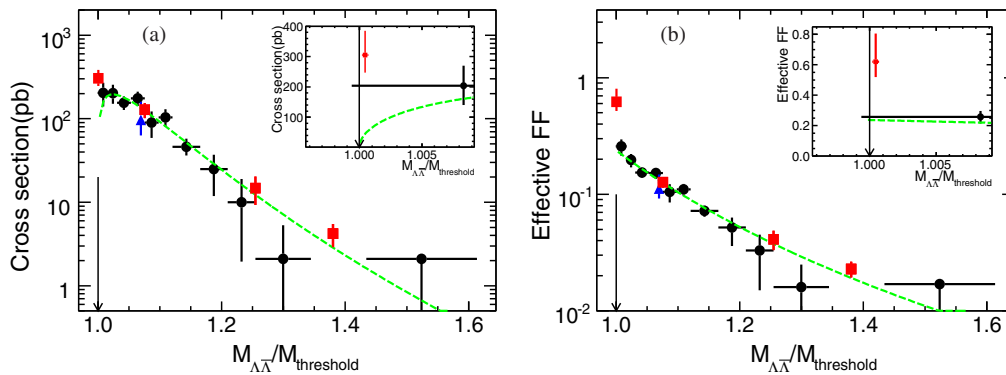


FIG. 3. Comparisons of (a) the Born cross section and (b) effective FF in this analysis with previous experiments for $\Lambda\bar{\Lambda}$ masses from 2.0 to 3.6 GeV/c^2 . The squares (red) represent the results from this analysis, the dots (black) and triangles (blue) are those from *BABAR* and *DM2* results. The dotted lines (green) are a phenomenological fit according to a pQCD prediction, the dotted vertical lines indicate the threshold. The insert plots are the zoomed-in results near threshold.

The results in this analysis may help to understand the mechanism of baryon production and test the theory hypotheses based on the threshold enhancement effect.

ACKNOWLEDGMENTS

The BESIII Collaboration thanks the staff of BEPCII, the IHEP computing center and the supercomputing center of USTC for their strong support. This work is supported in part by National Key Basic Research Program of China under Contract No. 2015CB856700; National Natural Science Foundation of China (NSFC) under Contracts No. 11235011, No. 11322544, No. 11335008, No. 11425524, No. 11635010; the Chinese Academy of Sciences (CAS) Large-Scale Scientific Facility Program; the CAS Center for Excellence in Particle Physics (CCEPP); the Collaborative Innovation Center for Particles and Interactions (CICPI); Joint Large-Scale Scientific Facility Funds of the NSFC and CAS under Contracts No. U1232201, No. U1332201, No. U1532257,

No. U1532258; CAS under Contracts No. KJCX2-YW-N29, No. KJCX2-YW-N45; 100 Talents Program of CAS; National 1000 Talents Program of China; INPAC and Shanghai Key Laboratory for Particle Physics and Cosmology; German Research Foundation DFG under Contracts No. Collaborative Research Center CRC 1044, No. FOR 2359; Istituto Nazionale di Fisica Nucleare, Italy; Koninklijke Nederlandse Akademie van Wetenschappen (KNAW) under Contract No. 530-4CDP03; Ministry of Development of Turkey under Contract No. DPT2006K-120470; National Natural Science Foundation of China (NSFC) under Contract No. 11505010; The Swedish Research Council; U.S. Department of Energy under Contracts No. DE-FG02-05ER41374, No. DE-SC-0010504, No. DE-SC-0010118, No. DE-SC-0012069; U.S. National Science Foundation; University of Groningen (RuG) and the Helmholtzzentrum fuer Schwerionenforschung GmbH (GSI), Darmstadt; WCU Program of National Research Foundation of Korea under Contract No. R32-2008-000-10155-0.

-
- [1] N. Cabibbo and R. Gatto, *Phys. Rev.* **124**, 1577 (1961).
 [2] J. Schwinger, *Particle, Sources, and Fields* (Perseus Books Publishing, Massachusetts, 1998), Vol. 3.
 [3] A. B. Arbuzov and T. V. Kopylova, *J. High Energy Phys.* **04** (2012) 009.
 [4] B. Delcourt *et al.* (DM1 Collaboration), *Phys. Lett. B* **86**, 395 (1979).
 [5] D. Bisello *et al.* (DM2 Collaboration), *Nucl. Phys.* **B224**, 379 (1983); *Z. Phys. C* **48**, 23 (1990).
 [6] A. Antonelli *et al.* (FENICE Collaboration), *Nucl. Phys.* **B517**, 3 (1998).
 [7] T. K. Pedlar *et al.* (CLEO Collaboration), *Phys. Rev. Lett.* **95**, 261803 (2005).
 [8] J. P. Lees *et al.* (BABAR Collaboration), *Phys. Rev. D* **87**, 092005 (2013); *Phys. Rev. D* **88**, 072009 (2013).
 [9] M. Ablikim *et al.* (BESIII Collaboration), *Phys. Rev. D* **91**, 112004 (2015).
 [10] G. Bardin *et al.* (PS170 Collaboration), *Nucl. Phys.* **B411**, 3 (1994).
 [11] T. A. Armstrong *et al.* (E760 Collaboration), *Phys. Rev. Lett.* **70**, 1212 (1993).
 [12] M. Ambrogiani *et al.* (E835 Collaboration), *Phys. Rev. D* **60**, 032002 (1999); M. Andreotti *et al.*, *Phys. Lett. B* **559**, 20 (2003).
 [13] M. N. Achasov *et al.*, *Phys. Rev. D* **90**, 112007 (2014).
 [14] D. Bisello *et al.* (DM2 Collaboration), *Z. Phys. C* **48**, 23 (1990).
 [15] B. Aubert *et al.* (BABAR Collaboration), *Phys. Rev. D* **76**, 092006 (2007).
 [16] S. Dobbs, A. Tomaradze, T. Xiao, K. K. Seth, and G. Bonvicini, *Phys. Lett. B* **739**, 90 (2014).
 [17] M. Ablikim *et al.* (BESIII Collaboration), [arXiv: 1710.00150](https://arxiv.org/abs/1710.00150).
 [18] O. D. Dalkarov, P. A. Khakhulin, and A. Y. Voronin, *Nucl. Phys.* **A833**, 103 (2010); B. El-Bennich, M. Lacombe, B. Loiseau, and S. Wycech, *Phys. Rev. C* **79**, 054001 (2009); J. Haidenbauer, H.-W. Hammer, U.-G. Meissner, and A. Sibirtsev, *Phys. Lett. B* **643**, 29 (2006); H. Fonvieille and V. A. Karmanov, *Eur. Phys. J. A* **42**, 287 (2009); L. Zhao, N. Li, S. L. Zhu, and B. S. Zou, *Phys. Rev. D* **87**, 054034 (2013); J. Haidenbauer and U. G. Meißner, *Phys. Lett. B* **761**, 456 (2016).
 [19] R. Baldini, S. Pacetti, A. Zallo, and A. Zichichi, *Eur. Phys. J. A* **39**, 315 (2009).
 [20] M. Ablikim *et al.* (BESIII Collaboration), *Nucl. Instrum. Methods Phys. Res., Sect. A* **614**, 345 (2010).
 [21] S. Agostinelli *et al.* (GEANT4 Collaboration), *Nucl. Instrum. Methods Phys. Res., Sect. A* **506**, 250 (2003).
 [22] Z. Y. Deng *et al.*, *Chin. Phys. C* **30**, 371 (2006).
 [23] D. J. Lange, *Nucl. Instrum. Methods Phys. Res., Sect. A* **462**, 152 (2001); R. G. Ping *et al.*, *Chin. Phys. C* **32**, 599 (2008).
 [24] R. G. Ping, *Chin. Phys. C* **38**, 083001 (2014).
 [25] C. M. Carloni Calame, *Phys. Lett. B* **520**, 16 (2001).
 [26] J. C. Chen, G. S. Huang, X. R. Qi, D. H. Zhang, and Y. S. Zhu, *Phys. Rev. D* **62**, 034003 (2000).
 [27] K. A. Olive *et al.* (Particle Data Group), *Chin. Phys. C* **38**, 090001 (2014).
 [28] C. Bernardini, G. F. Corazza, G. Di Giugno, G. Ghigo, J. Haissinski, P. Marin, R. Querzoli, and B. Touschek, *Phys. Rev. Lett.* **10**, 407 (1963).
 [29] A. Hoecker *et al.*, *Proc. Sci.*, ACAT2007 (2007) 040.

- [30] The energy seed is the calorimeter channel with the maximum energy deposit among its neighbor calorimeter channels within one cluster. The *second moment* is defined as $\sum_i^n E_i r_i^2 / \sum_i^n E_i$, and the *lateral moment* is defined as $\sum_{i=3}^n E_i r_i^2 / (E_1 r_0^2 + E_2 r_0^2 + \sum_{i=3}^n E_i r_i^2)$, where $r_0 = 5$ cm is the average distance between adjacent crystal centers, r_i is the radial distance of crystal i from the cluster center, and E_i is the crystal energy in decreasing order. The *deposition shape* is defined as $(E_{5 \times 5} - E_{3 \times 3}) / E_{5 \times 5}$, where $E_{3 \times 3}$ and $E_{5 \times 5}$ are the deposited energies in 3×3 and 5×5 crystals around the seed energy, respectively.
- [31] X. Zhou, Overview of QCD studies at BESIII, in *Proceedings of Excited QCD, Sintra, Portugal, 2017* (2017).
- [32] N. Berger, Z.-A. Liu, D.-P. Jin, H. Xu, W.-X. Gong, K. Wang, and G.-F. Cao, *Chin. Phys. C* **34**, 1779 (2010).
- [33] M. Ablikim *et al.* (BESIII Collaboration), arXiv: 1702.04977.
- [34] G. D'Agostini, *Nucl. Instrum. Methods Phys. Res., Sect. A* **346**, 306 (1994).
- [35] M. Ablikim *et al.* (BESIII Collaboration), *Phys. Rev. D* **89**, 074039 (2014).
- [36] S. Pacetti, R. B. Ferroli, and E. Tomasi-Gustafsson, *Phys. Rep.* **550–551**, 1 (2015).